Available online at www.sciencedirect.com
ScienceDirect
Ceramics International 35 (2009) 3339–3346
CERAMICS INTERNATIONAL
www.elsevier.com/locate/ceramint

Surface strength of silicon nitride in relation to rolling contact performance

Wei Wang [a], Mark Hadfield [a,*], Andrew A. Wereszczak [b]

[a] School of Design, Engineering and Computing, Bournemouth University, Poole, BH12 5BB, United Kingdom
[b] Materials Science and Technology Division, Oak Ridge National Laboratory, Oak Ridge, TN 37831, United States

Received 10 April 2009; received in revised form 27 April 2009; accepted 27 May 2009
Available online 7 July 2009

Abstract

Silicon nitride material has been traditionally used as bearing material due to its superior performance against bearing steel. Its successful application as a bearing element has led to the development of rolling contact applications in turbomachinery and automotive industries. In the case of latter, this is especially true for the engine manufacturing industry where its excellent rolling contact performance can make significant savings on warranty cost for engine manufactures. In spite of these advantages, the remaining limitation for their broader application is the high component machining cost. Further understanding of rolling contact performance of silicon nitride in relation to its surface integrity will enable engine manufacturers to produce components that meet the design requirements while at the same time reduce the machining cost. In the present study, the relationship between the C-sphere strength of a silicon nitride and its rolling contact fatigue life is investigated. The C-sphere test is used here to compare the strengths of three batches of sintered reaction-bonded silicon nitride (SRBSN) specimens with different subsurface quality induced by variation of machining parameters. In parallel, the rolling contact fatigue (RCF) performance of those machining conditions is studied on a modified four-ball tester. The results show that the most aggressively machined specimens have the weakest C-sphere strength and the shortest RCF life. This positive relationship can give component manufacturers a valuable reference when they make selections of candidate material and finishing standards.

Keywords: Rolling contact; Ceramics; Silicon nitride; Surface strength; Flexure strength

1. Introduction

Silicon nitride (Si_3N_4) has been widely used as rolling contact element in hybrid and all ceramic bearings for its superior performance against bearing steels. Its successful application as bearing elements leads to the development of silicon nitride in rolling contact applications in automotive, turbomachinery and power industries. It has a significant advantage due to its low density (less than half of bearing steel), low friction, corrosion resistance and good performance under extreme condition [1]. There are a number of Si_3N_4 engine components are now in commercial production, however, the limiter to their broader application is high machining cost, which accounts for 55–70% of final component cost for different types of component [2]. Further understanding of rolling contact performance of Si_3N_4 material in relation to its surface integrity will enable engine manufacturers to produce components that meet the design requirements while minimizing their machining cost.

2. Silicon nitride material and specimen preparation

Si_3N_4 has been developed for over half a century, and during this period, its mechanical property has been significantly improved. There are many processing methods used in industry to fabricate Si_3N_4, and among them, there are two typical processing routes, reaction-bonding and hot isostatically pressing. Reaction-bonded silicon nitride (RBSN) processing is a method to produce Si_3N_4 material through incorporation and nitridation of silicon powders, which was mainly developed in the 1950s [3]. A major problem associated with RSBN material is its low density and high porosity, which often is a cause of its low strength. The hot isostatically pressing (HIP) method has then developed to produce Si_3N_4 with higher density and lower porosity. It uses Si_3N_4 powders as raw material and various sintering additives to produce bulk Si_3N_4 in a confined space of graphite die under a hot, nitrogen environment. HIPed Si_3N_4 has much better strength than RBSN

* Corresponding author. Tel.: +44 (0)1202 965983; fax: +44 (0)1202 965314.
E-mail address: mhadfield@bournemouth.ac.uk (M. Hadfield).

0272-8842/$36.00
doi:10.1016/j.ceramint.2009.05.034

Si_3N_4, but its high material cost prevents its attraction to more widespread applications. In an effort to combine the advantage of low cost of RBSN and high strength of HIPed Si_3N_4, the sintered reaction-bonded silicon nitride (SRBSN) was developed. It produces Si_3N_4 by post-sintering the reaction-bonded silicon nitride. It can achieve a relatively high strength at a fraction of fabrication cost of HIPed Si_3N_4.

Ceralloy 147-31N (Ceradyne, USA) SRBSN is investigated in this study due to the commercial potential of SRBSN for bearing applications. Ceralloy 147-31N Si_3N_4 is a typical SRBSN that has been used in mass production of a range of diesel engine components, including fuel injector cam roller follower and link pin, fuel pump roller and exhaust valve cam roller follower. They have superior rolling contact performance compared with steel components and that enables engine manufacturers to reduce warranty cost. However there is insufficient knowledge on contact reliability of Ceralloy 147-31N Si_3N_4, and how machining affects that, so the intent was to address this in this study.

The micrographs of a Ceralloy 147-31N Si_3N_4 specimen are shown in Fig. 1. The microstructure is polished using diamond suspension, and the size of the diamond paste used in the suspension is gradually reduced from 15 μm to 1/4 μm. The polished surface is plasma etched using a mixture of carbon fluoride and oxygen for 6.5 min before it is coated for SEM examination. The darker grey phase in the microstructure is β-Si_3N_4, which is the major constituent phase in the microstructure. The lighter grey phase, which can be found between the grains boundary is a glassy phase, which is formed by sintering aides (rare earth oxides). The needle-like grains interlock with each other, which are thought to be responsible of improving fracture toughness. However, the relatively long length of the needle-like grains can limit the strength of the material, so a compromise must be struck between desired fracture toughness and strength.

In order to examine the relationship between rolling contact performance of Ceralloy 147-31N Si_3N_4 and its surface integrity, the as-sintered ingot was machined into three batches (with ten specimens in each batch) of 12.7 mm diameter balls each having different machining parameters. Table 1 shows the applied machining procedures. These three conditions are referred as coarse, fine and conventional conditions. Roughing, the first step of three step grinding process are the same for all three conditions. The second step of the grinding process was intended to produce different depths of machining damage in the ball's near-surface-volume. The variation on the second step produces Si_3N_4 ball specimens with different subsurface qualities, such as the depth of subsurface damage, population of the micro-cracks, etc. The final step of grinding guarantees that coarse and fine specimens have the same surface roughness. The conventional specimens have a better surface finish by introducing 1200 grit diamond paste on the final finish. Five balls in each batch were tested on a modified four-ball tester to compare their rolling contact fatigue performance, and the other five balls in each batch were machined into C-sphere test specimen to examine the variation in hoop tensile strength caused by grinding. The design consideration, the geometry of the C-sphere and the loading scenario are explained in the next section.

Table 1
Machining procedures applied to finish 12.7 mm diameter ball specimens.

Specimen type	Finishing step	Diamond size	Removal
Coarse	1 (Roughing)	Accepted practice	
	2 (Induce damage)	100 grit	0.1000 mm
	3 (Finishing)	600 grit	0.0127 mm
Fine	1 (Roughing)	Accepted practice	
	2 (Induce damage)	180 grit	0.1000 mm
	3 (Finishing)	600 grit	0.0127 mm
RCF-conventional	Use the "accepted" practice for RCF finishing (using 180, 220, 320 grit diamond, and 600 and 1200 grit diamond paste in sequence)		

3. C-sphere test

A C-sphere flexure strength test specimen was developed to enable the study of and measurement of surface strength and linked flaw size [4]. The design of the C-sphere specimen was inspired by the C-ring specimen, which is used to evaluate the

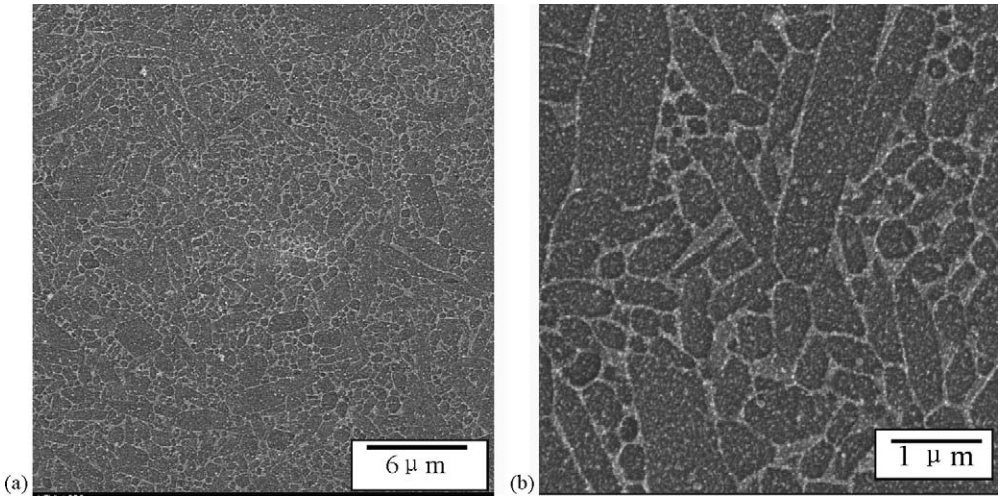

Fig. 1. Microstructure of Ceralloy 147-31N SRBSN after plasma etching.

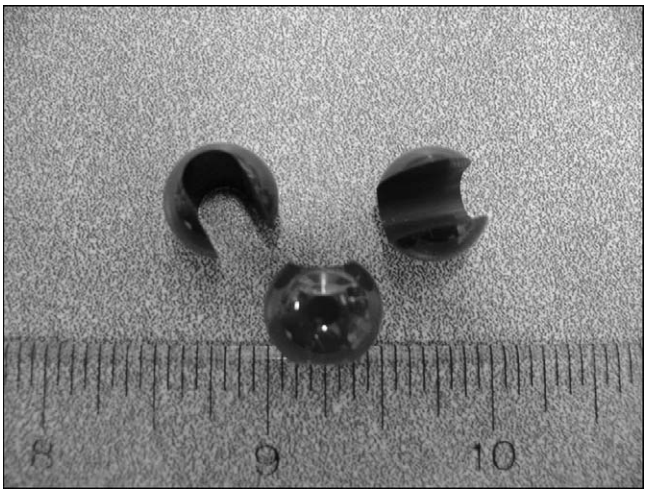

Fig. 2. Pre-test C-sphere specimens.

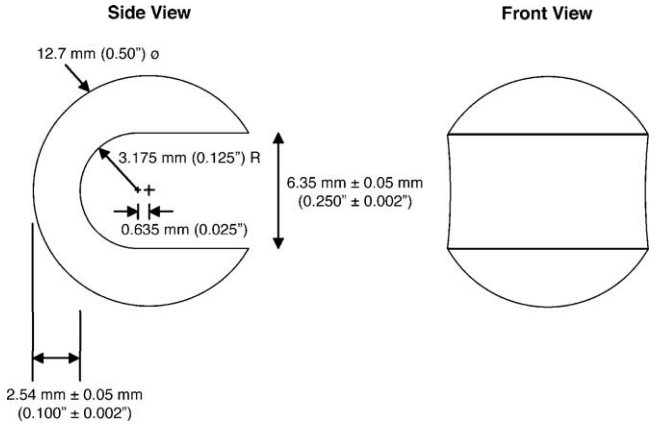

Fig. 3. C-sphere specimen geometry.

strength of ceramic tubes [5]. Enabling the identification of a flaw type (usually surface- or near-surface-located) and measurement of its size in finished ceramic balls is obviously important for the study of strength, but perhaps more importantly, for the study and predictability of RCF performance (a response limited by surface- or near-surface-located flaws or in changes thereof).

Three batches of Ceralloy 147-31N Si_3N_4 balls with a diameter of 12.7 mm, as described in Table 1 were machined into C-sphere flexure strength specimens, which are shown in Fig. 2. Grinding of the slot was performed in a two step process using a Type 1F1 diamond plated grinding wheel (127 mm diameter × 6.35 mm thick × 3.175 mm *R*) for the final grinding. The geometry and tolerance of the C-sphere specimen is shown in Fig. 3. The design of the C-sphere geometry and its produced stress state are considered using an ANSYS finite element model. As shown in Fig. 4, the maximum stress occurs at the centre of the outer fibre. C-sphere flexure specimens were monotonically and compressively loaded to failure using an electromechanical universal testing machine at a crosshead displacement rate of 0.5 mm/min. The loading scenario is shown in Fig. 5. A special jig was used to horizontally align the C-sphere slot prior to loading. Load to fracture was recorded and combined with the failure load-failure stress relationship from FEA to determine C-sphere flexure strength. Weibull strength distributions were determined using commercially available software. Optical fractography was also conducted on all specimens to identify failure location and the fracture surfaces of a select few specimens were examined with SEM.

4. Rolling contact fatigue test of Si_3N_4 balls with artificial cracks

Bearing grade HIPed Si_3N_4 has excellent RCF, however, the RCF performance of SRBSN is less understood. In order to compare the RCF lifetime of coarse, fine, conventional Ceralloy 147-31N Si_3N_4 balls, artificial cracks are created and positioned into the contact path to accelerate the failure of the test specimens. A modified Plint TE 15 impact tester is used to generate the surface cracks. A test Si_3N_4 specimen is attached to a pendulum, and released at 60° angle to collide with a fixed contact ball. The energy absorbed during the contact can be calculated by the potential energy loss of the pendulum. The contact ball used for the artificial crack generation is TSN-03H HIPed Si_3N_4. Fig. 6 shows the artificial crack under ultra-violet (UV) light after dye penetration. Fig. 7 shows SEM image of the centre of the crack where the two crack edges have an approximate gap of 2.5 μm.

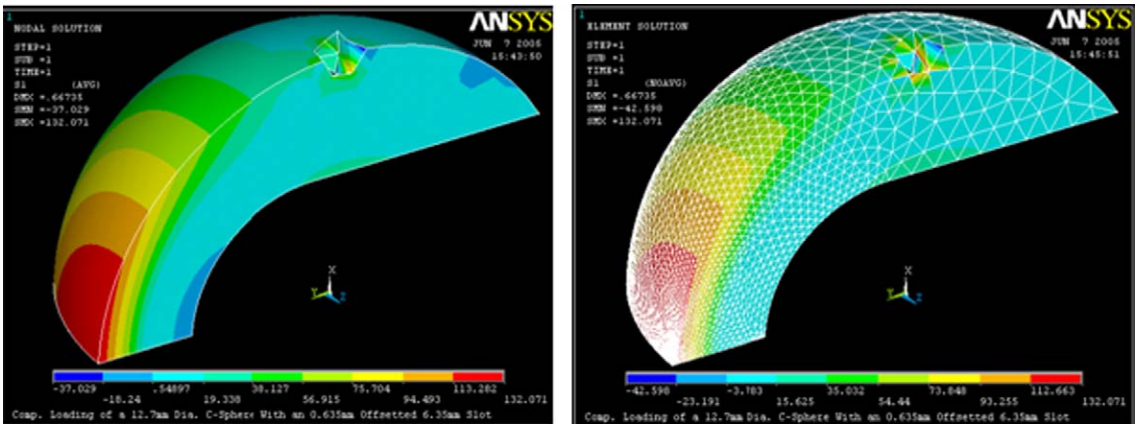

Fig. 4. ANSYS analysis of C-sphere geometry.

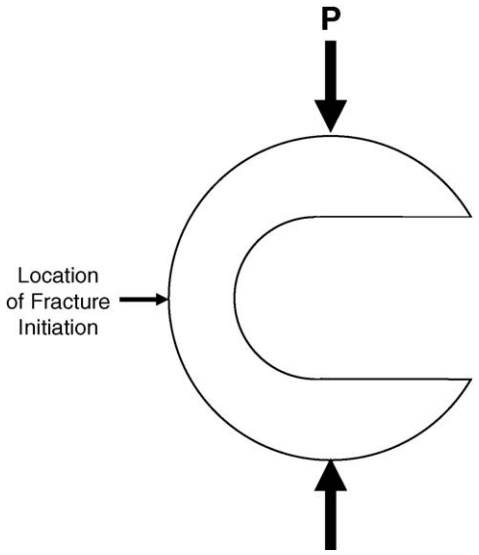

Fig. 5. Loading scenario of C-sphere test.

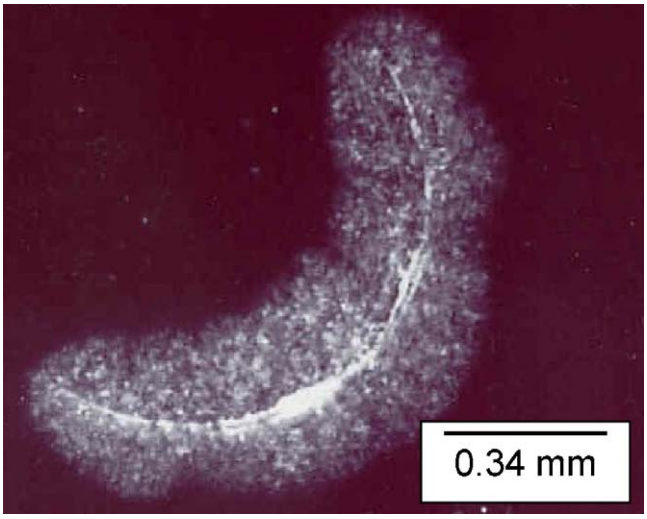

Fig. 6. Visualizing crack under UV light after dye treatment.

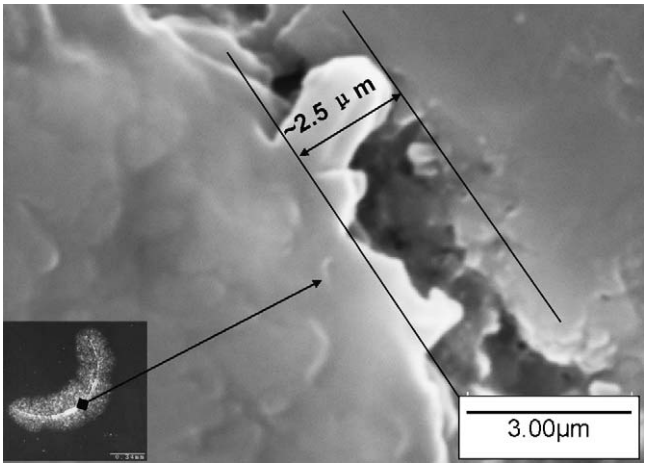

Fig. 7. Approximate crack gap size measured in SEM examination.

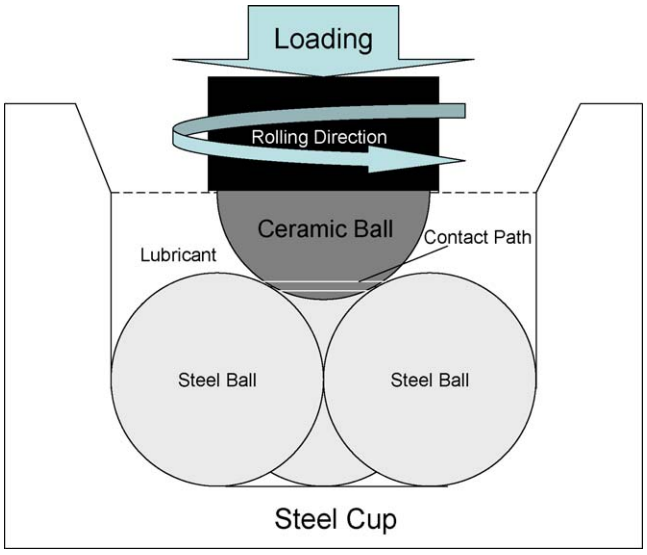

Fig. 8. Schematic of modified four-ball test – contact geometry.

A modified four-ball machine is used to perform the test [6]. Fig. 8 shows the schematic of modified four-ball contact with Si_3N_4 fixed in the collet as upper driving ball and three steel balls in the cup as lower contact balls. The centre of contact path on the upper Si_3N_4 ball situates at 1.17 mm above the bottom of the ball. In order to classify the position of the crack within the contact path, the positioning parameters of the crack, and some typical positions of the crack are shown in Fig. 9 [7]. As shown in the schematic, β measures the angle between ring crack and the contact path centre line. $2a$ is the width of the contact path, and R represents the radius of the ring crack. δ measures the distance between the centre of the hypothetic ring crack circle and the centre line of the contact path. For all the tests, Castrol 75w90 transmission oil is selected as the lubricant due to the chemical compatibility, potential automotive application of the Si_3N_4 bearing and the lubricant's relatively high viscosity to maintain a lubrication

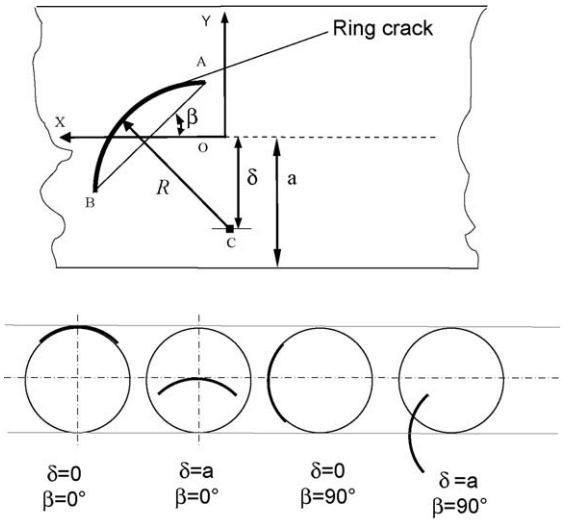

Fig. 9. Crack positioning parameter and typical locations of the crack.

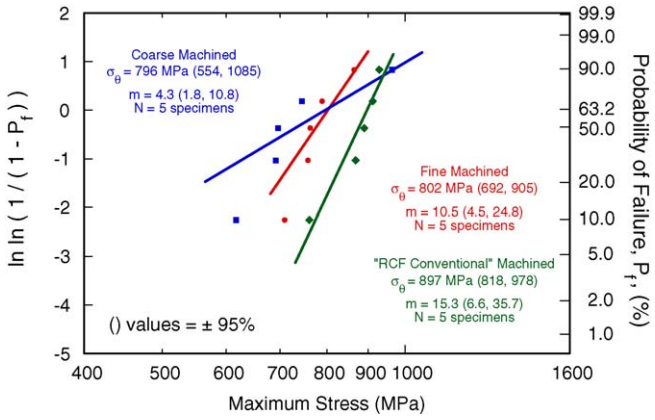

Fig. 10. Weibull analysis of C-sphere strength. Values in parentheses represent ±95% confidence interval.

film to reduce the contact between silicon nitride surface asperity and the steel ball surface. The applied Hertzian contact stress between the upper ball and lower balls is 5.6 GPa, and the spindle speed is 5000 rpm, which results in 11,250 stress cycle/min.

5. Results and discussion

5.1. C-sphere strength

Five C-Sphere specimens machined from each of three batches of coarse, fine and conventional balls were tested. The maximum stress is calculated in ANSYS from the mechanical load used to break the specimens. The two-parameter Weibull analysis of the results is show in Fig. 10. There is a trend of increasing characteristic strength from coarse, fine to conventional conditions. The coarse specimen has a characteristic strength of 796 MPa, while fine and conventional specimens have strengths of 802 and 897 MPa, respectively. The fracture surface of a tested C-sphere specimen is shown in Figs. 11 and 12. Fig. 11 shows a typical fractography of a ceramic fracture surface, where the fracture origin is identified. The magnified fracture origin is shown in Fig. 12. According to the C-sphere fractography, the fracture origin is mostly on the surface, sometimes in the near-surface area, although it is not necessary to appear on the maximum stress area on the centre of outer fibre of C-sphere specimen. According to Griffith's Criterion, for a fracture toughness of 6 MPa $\sqrt{m}$ and crack geometry factor of 1.5, the estimate strength-limiting flaw sizes are around 27.9, 27.6 and 22.1 μm for coarse, fine and conventional conditions, respectively. This result reflects the machining effect on the surface/subsurface integrity of the specimens. Aggressive machining is perceived to generate deeper subsurface damage and higher population of micro-cracks, which are considered to act as one type of the strength-limiting flaw. This perception is preliminarily verified by C-sphere flexure test, however, more tests should be done to make such a statistically confident conclusion.

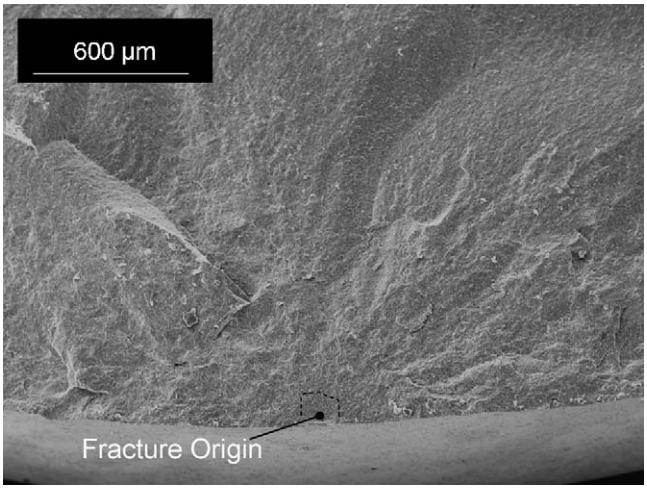

Fig. 11. Fractography of Si_3N_4 fracture surface.

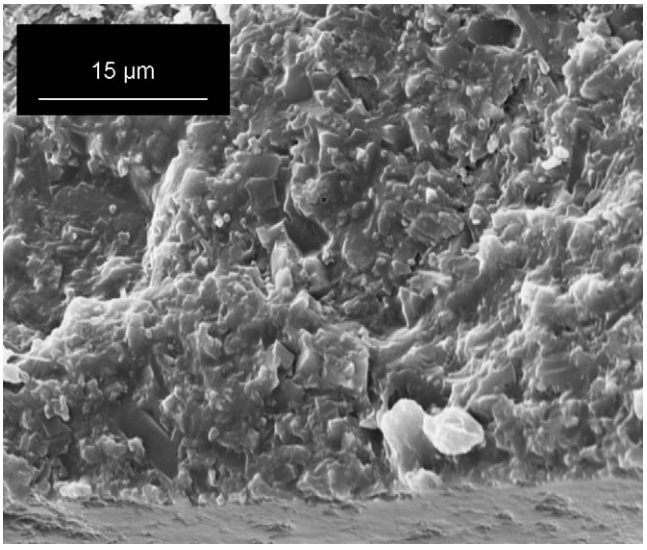

Fig. 12. Fracture origin.

Table 2
RCF results of Ceralloy 147-31N SRBSN.

Specimen ID	Crack position parameter (β)	Crack position parameter (δ)	Fatigue life (no. of stress cycles)
Coarse-01	90°	0	2×10^5
Coarse-02	90°	0	3.7×10^5
Coarse-03	90°	0	2.3×10^5
Coarse-04	90°	0	4×10^5
Coarse-05	90°	0	3.3×10^5
Fine-01	90°	0	4.1×10^5
Fine-02	90°	0	3.0×10^5
Fine-03	90°	0	4.2×10^5
Fine-04	90°	0	3.4×10^5
Fine-05	90°	0.5a	1.2×10^7
Conventional-01	90°	0	4.8×10^5
Conventional-02	90°	0	8×10^5
Conventional-03	90°	0	1.5×10^6
Conventional-04	90°	0	4.5×10^5
Conventional-05	45°	0.5a	Suspended

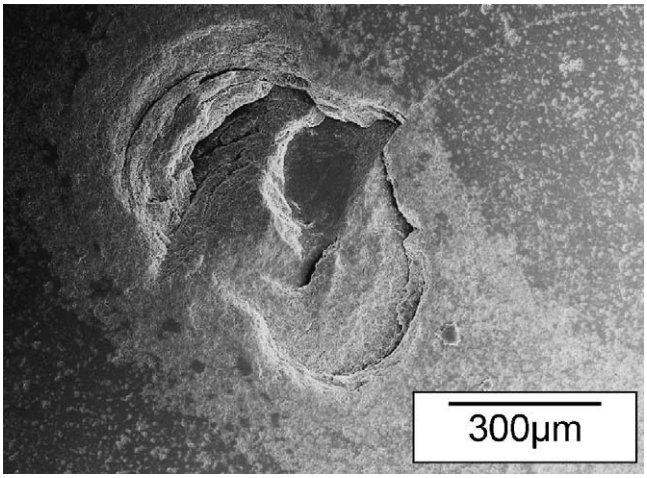

Fig. 13. Spall profile of specimen Fine-05.

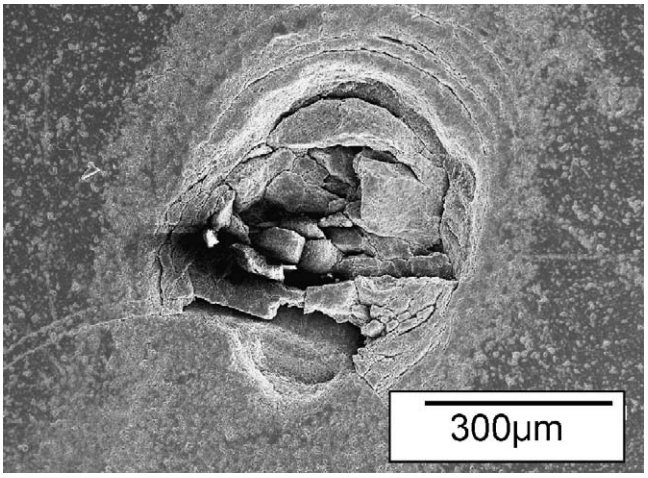

Fig. 16. Spall profile of specimen Fine-02.

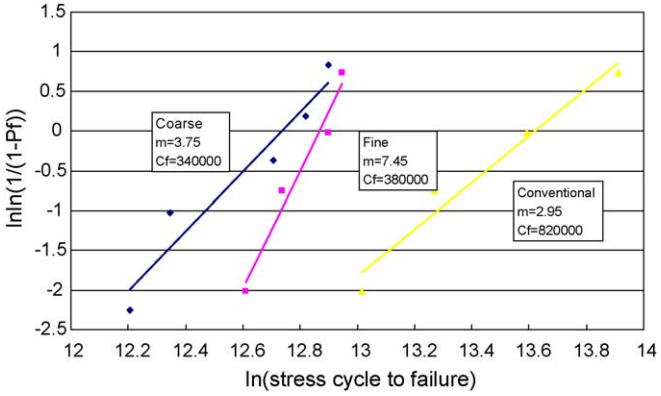

Fig. 14. Weibull analysis of RCF test results of coarse, fine and conventional conditions.

5.2. RCF test

Five balls in each batch of coarse, fine and conventional conditions are tested, and their fatigue lifetimes relative to the positioning parameters are summarised in Table 2. There are two specimens Fine-05 and Conventional-05, which are not positioned accurately in the contact path. The SEM image illustrating the crack position of Fine-05 specimen is shown in Fig. 13. As shown in the image, only the tip of the crack is positioned in the contact path instead of the centre of the crack, which results in an extended fatigue life of 1.2×10^7 stress cycles. Considering the RCF results of other specimens with positioning parameter $\delta = 0$, $\beta = 90^\circ$, the number of stress cycles to failure are mostly in the order of 10^5. Compared with these results, the RCF life of Fine-05 specimen is extended around 50–100 times, indicating the importance of artificial crack positioning on RCF life of Si_3N_4. For this reason, these two specimens are excluded from Weibull analysis. From the Weibull analysis results shown in Fig. 14, we can see that conventional specimens show an extended lifetime compared with fine and coarse specimen with identical artificial crack on the surface and cracks positioned in the contact path with the same positioning parameter. The coarse specimen has the worst RCF performance, with a characteristic stress cycles to failure $C_f = 3.4 \times 10^5$. However, in order to improve the reliability of RCF results, more tests should be run to give a statistically

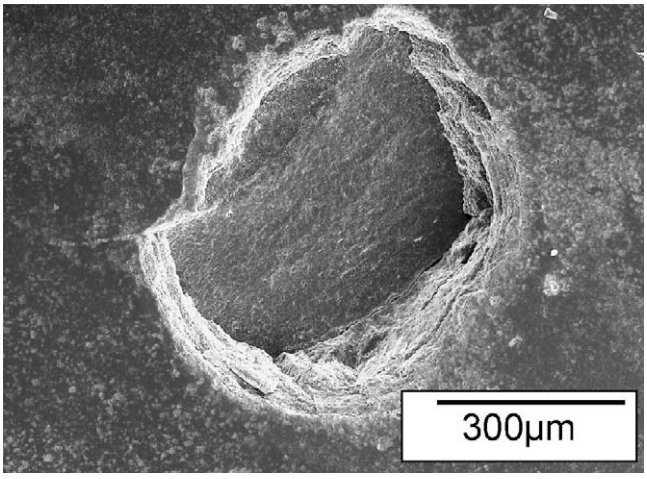

Fig. 15. Spall profile of specimen Coarse-01.

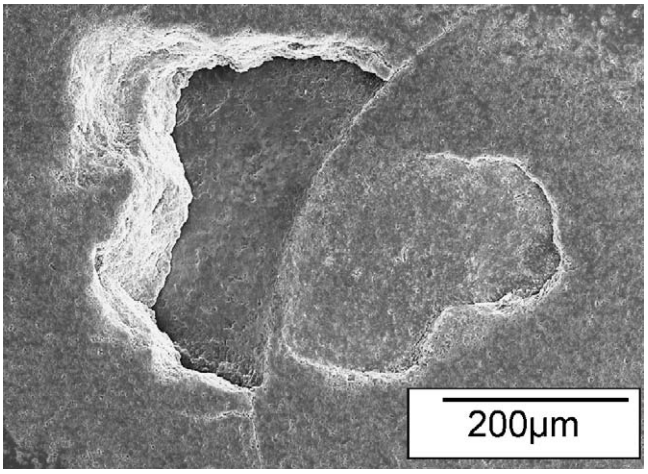

Fig. 17. Spall profile of specimen Conventional-02.

confident conclusion. Figs. 15–17 shows the spall profile of specimens Coarse-01, Fine-02 and Conventional-02, respectively. Although there are variations on the geometry of the spalls from specimen to specimen, there is evidence that secondary cracks are developed in the spalling process (Fig. 17).

5.3. The correlation between RCF and C-sphere test results

The C-sphere and RCF tests reveal the same trend of increasing strength and fatigue life of coarse, fine and conventional specimens. This correlation can be explained by the analysis of stress field of C-sphere specimen and four-ball contact. The failure of the C-sphere specimen is perceived to be micro-crack propagation when the outer fibre is subject to tensile stress. The tensile stress field of the outer fibre was previously shown in Fig. 4. During the specimen machining process, coarse specimens are the most aggressively machined, which result in a higher density and greater depth of induced micro-cracks. As described earlier, the size of the flaw where fracture initiates determine the strength of C-sphere. For the coarse condition, there is a higher probability that deeper strength-limiting flaws (micro-cracks) are located at the maximum tensile stress area, and the size of the flaw cause a weaker strength of coarse C-sphere specimen.

In modified four-ball test, the upper Si_3N_4 ball is subject to Hertzian contact against the contact ball. For a perfect Si_3N_4 ball without any surface cracks (natural or artificial) positioned in the contact path, the maximum tensile stress generated on the surface due to Hertzian contact is not high enough to initiate a crack. As a result, the RCF life for a perfect Si_3N_4 ball is very long, and it does not normally fail within a reasonable testing time (100 million stress cycles). However, for a pre-cracked Si_3N_4 ball, due to the existing of an artificial crack, the stress field on the surface is changed, which is explained in Fig. 18-b. There is a gap existing between the two crack edges. For the type of artificial cracks created in the RCF tests in this study, as described earlier, the width of the gap is measured at 2.5 μm. As a result of the gap, when the section of the ball surface to the left of the crack is subject to contact stress, it creates a bending force which generates a tensile stress field on the specimen surface. Together with the stress field created due to Hertzian contact, when the overall tensile stress on the surface reaches a threshold, the micro-cracks will propagate to form a secondary crack on the surface. Due to the existence of a secondary crack, it created a tertiary crack under a similar scenario, and so on so forth, as illustrated in Fig. 18-a. The secondary and tertiary crack propagates to meet the original crack and meet each other, which form a spall type of failure. Fig. 19 shows the secondary cracks of Fine-02 specimen and associated spall failure. The mechanism of forming a secondary crack on the surface in modified four-ball test is quite similar to micro-crack propagation in C-sphere test when it is interpreted by tensile stress on the surface, which explains the correlation between RCF results and C-sphere results. The boundary element modelling of the artificial crack under Hertzian pressure was carried out by Wang and Hadfield, and the simulation results show the same conclusion [8,9].

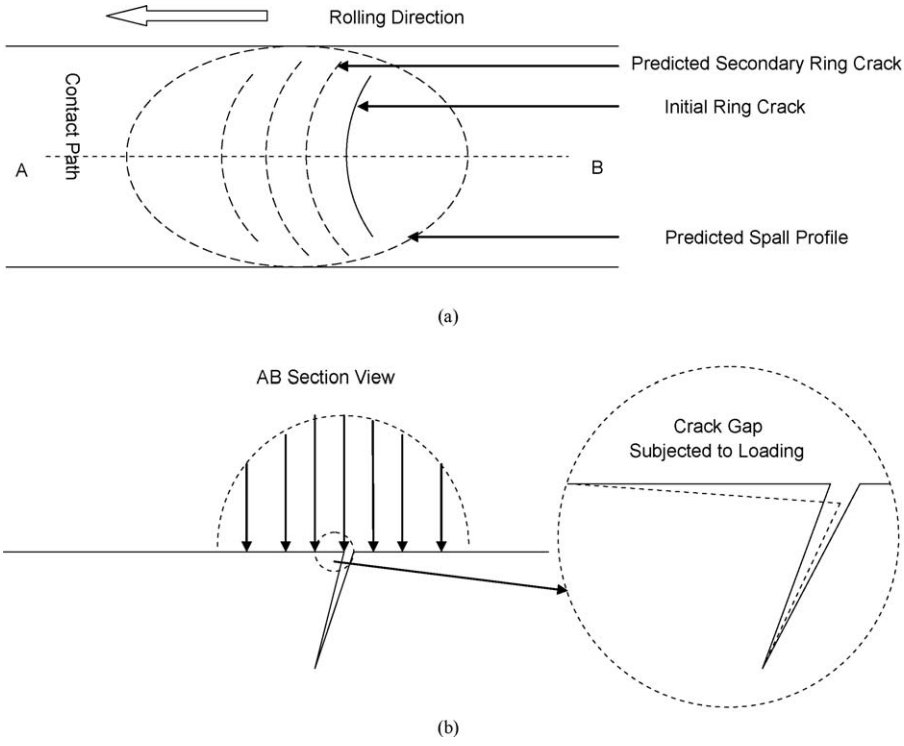

Fig. 18. (a) Location of original crack and secondary cracks in the contact path; (b) mechanism of secondary crack creation.

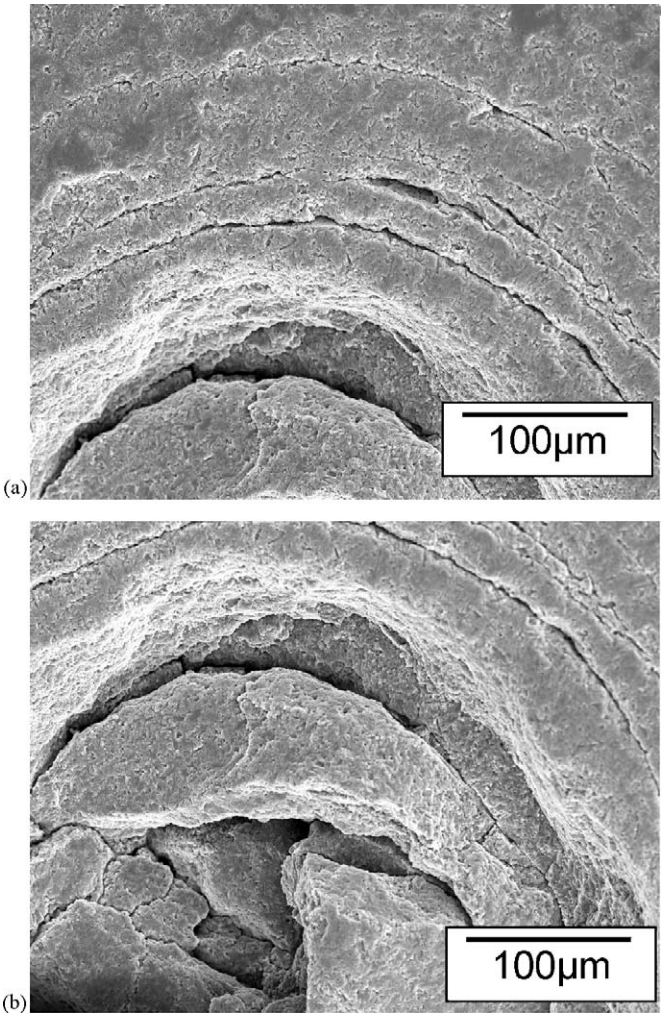

Fig. 19. Secondary cracks created on the surface of Fine-02 specimen.

6. Conclusion

I. The C-sphere flexure strength results of Ceralloy 147-31N SRBSN show an increased strength comparing from coarsely, fine to conventionally machined conditions.

II. The RCF result reveals an increasing fatigue lifetime among three batches of specimens with the subsurface finished to coarse, fine and conventional condition. The conventional condition shows the longest rolling contact fatigue life, however, the coarse condition has the shortest lifetime under the same test condition.

III. The trend of C-sphere and rolling contact fatigue results are explained by the similarity of the tensile stress field created in C-sphere and rolling contact fatigue test which result in the eventual failure. Due to the positive relationship between C-sphere and rolling contact fatigue results, C-sphere strength can be used as a predictor of fatigue lifetime of Si_3N_4 balls. It can help designers to screen out ''weak'' candidate silicon nitride material prior to rolling contact fatigue test, which can make reasonable savings on time and cost. Additionally, because flaw types can be identified, C-sphere strength testing can be used by Si_3N_4 manufactures and ball finishers to assess the quality of their product.

Acknowledgements

The authors wish to acknowledge Oak Ridge National Laboratory in United States for funding this project, and ETC in Brunel University in United Kingdom for help on SEM examination.

References

[1] Y. Wang, M. Hadfield, ASM Handbook, vol. 11, 2002, pp. 957–964.
[2] U. Effner, M. Woydt, Slip-rolling and machining of engineering ceramics, in: Research Report 259, BAM, Berlin, 2002.
[3] F.L. Riley, Journal of the American Ceramic Society 83 (2000) 245–265.
[4] A.A. Wereszczak, W. Wang, O.M. Jadaan, T.M. Kirkland, Ceramic Science and Engineering Proceedings 27 (2006) 281–293.
[5] C1323, Annual Book of ASTM Standards, ASTM International, 2001, pp. 1–6.
[6] R. Tourret, E.P. Wright, Rolling Contact Fatigue Performance Testing of Lubricants: Papers Presented at The International Symposium Organized By the Institute of Petroleum, Heydon, London, 1976.
[7] Y. Wang, M. Hadfield, Wear 243 (2000) 157–166.
[8] Y. Wang, M. Hadfield, Wear 253 (2002) 975–985.
[9] Y. Wang, M. Hadfield, Wear 254 (2003) 597–605.